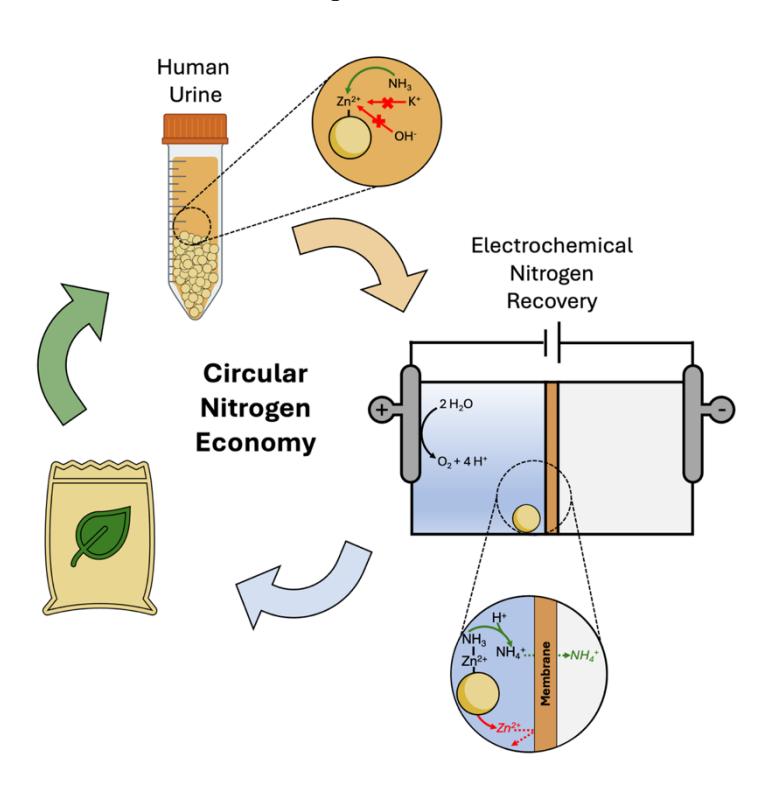
1	Enhancing Resource Recovery through Electro-Assisted Regeneration of an Ammonia-
2	Selective Cation Exchange Resin
3	Edward Apraku ¹ , Chloe M. Laguna ² , Robert M. Wood ¹ , Neha Sharma ^{2,3} , Hang Dong ⁴ , William
4	A. Tarpeh ^{1,2} *
5	¹ Department of Civil and Environmental Engineering, Stanford University, Stanford, CA, 94305,
6	United States
7	² Department of Chemical Engineering, Stanford University, Stanford, CA, 94305, United States
8	³ Stanford Synchrotron Radiation Lightsource, SLAC National Accelerator Laboratory, Menlo
9	Park, CA, 94025, United States
10	⁴ Georgia Tech Shenzhen Institute, Tianjin University, Shenzhen, Guangdong, 518055, China
11	*Corresponding author, Email: <u>wtarpeh@stanford.edu</u> Address: 443 Via Ortega, Room 387,
12	Stanford, CA, 94305, United States. Telephone: (650) 497-1324
13	Text: 6550 words
14	Figures: 7
15	
16	

Graphical Abstract



26 Abstract

27

28

29

30

31

32

33

34

35

36

37

38

39

40

41

42

Ammonia-selective adsorbents can manage reactive nitrogen in the environment and promote a circular nutrient economy. Weak acid cation exchangers loaded with zinc exhibit high ammonia selectivity but face two implementation barriers: the stability of the zinc-carboxylate bond in complex wastewaters and energy- and logistics-intensive adsorbent regeneration with acidic solutions. In this study, we examined the stability of the zinc-carboxylate bond in varying solutions (pure ammonium solution, synthetic urine, and real urine) and during electro-assisted regeneration. For electrochemical regeneration, both electrolyte concentration and current density influenced the tradeoff between ammonia regeneration and zinc elution. Using 10 mM K₂SO₄ anolyte at 0.08 mA/cm² current density, we achieved 4% zinc elution and 61% ammonia regeneration. In contrast, using 100 mM K₂SO₄ at 4.96 mA/cm² improved regeneration efficiency to 97% but eluted 60% of zinc. We found that the electrolyte concentration was the key factor influencing the regeneration efficiency of NH₃-selective adsorbents. Due to prevalent zinc elution, we designed an *in-situ* procedure for reforming the zinc-carboxylate bond and achieved similar adsorption densities between pre- and post-regenerated resin, thus enabling multiple cycle resin use. Ultimately, this study advances the understanding of ammonia-selective resins that can facilitate high-purity, selective, and durable nutrient recovery from waste streams.

- Keywords: adsorbent stability, ammonia selectivity, circular economy, electrochemical water splitting, nutrient recovery, water electrolysis
- 45 Synopsis: Electrified adsorbent regeneration can control the recovery efficiency and chemical
- stability of ammonia-selective adsorbents.

Introduction

Anthropogenic discharges (e.g., untreated wastewater and fertilizer runoff) have led to an imbalance of reactive nitrogen such as ammonium (NH₄+), ammonia (NH₃), and nitrate (NO₃-) in the environment. This imbalance has caused eutrophication, monetary loss from impacted recreation and tourism, and detrimental human health effects. The Haber-Bosch process, which converts inert atmospheric N₂ to ammonia for fertilizers, is a major contributor to this nitrogen imbalance and its environmental implications. This catalytic nitrogen fixation uses 1% of the world's total energy production and produces 1.4% of global CO₂ emissions. In contrast, exploring alternative nitrogen sources, such as wastewater, can reduce the dependency on Haber-Bosch derived fertilizers by recovering and repurposing reactive nitrogen. For example, urine accounts for 80% of the total nitrogen but only 1% of the volume in wastewater and contains concentrated levels of NH₃-nitrogen (often above 3,000 mg N/L). To promote a more sustainable nutrient economy and safeguard the environment from harmful algal blooms, effective management of reactive nitrogen species is necessary.

Contemporary nutrient mitigation techniques (e.g., biological methods, chemical precipitation) prioritize nutrient removal over recovery to satisfy the stringent discharge requirements of wastewater treatment plants. Nutrient recovery from urine could reduce nutrient removal costs (e.g., decreased sludge production) and provide supplemental fertilizers (e.g., struvite from phosphorus recovery, ammonium sulfate from recovery).⁵ Ion exchange (IX) resins are a viable approach for the effective management and recovery of nutrients from waste streams. Specifically, weak acid cation (WAC) exchange resins have potential as a low-cost, low-energy, modular technique for ammonium (NH₄⁺) recovery from urine by facilitating electrostatic binding

of NH₄⁺ to carboxylate functional groups.^{6,7} However, in real urine applications, WAC resins show a maximum NH₄⁺ adsorption capacity of 6 mmol N/g resin due to limited selectivity in multicomponent wastewaters containing competing cations (e.g., Na⁺, K⁺, Ca²⁺).^{8,9} Electrostatically loading zinc ions onto commercial WAC IX resins enhances selectivity towards total ammonium nitrogen (i.e., the sum of NH₄⁺ and NH₃, or TAN) through inner-sphere ammoniazinc interactions, which enable an intrinsic TAN/K⁺ selectivity of 10.1 (up to ten times higher than commercial resins).¹⁰ *Ex-situ* regeneration of these NH₃-selective resins with mild commercial acids (pH 3.25 to 4.25) achieved high TAN recovery (>90%).¹⁰ While these achievements are promising, chemical regeneration with commercial acids and bases limits implementation in water treatment systems. Producing chemical regenerants, such as sulfuric acid for cation exchange resins, accounts for up to 70% of treatment greenhouse gas emissions and energy input for adsorptive nitrogen recovery from wastewater.¹¹ To better justify the use of adsorbents for water treatment, nutrient technologies must mitigate the external chemical usage needed for regeneration.

Electro-assisted regeneration of IX resins could lower the emissions and energy input for chemical regeneration; however, *in-situ* electro-assisted regeneration of ammonia-selective adsorbents is underdeveloped. Electro-assisted regeneration uses either the acidic anode solution from the oxygen evolution reaction (OER) for cation exchange resins or the alkaline cathode solution from the hydrogen evolution reaction (HER) for anion exchange resins (**Figure S1**). An electrochemical-ion exchange (EC-IX) system integrating resin inside the reactor can facilitate *in-situ* regeneration of IX resins and simultaneous recovery of high-purity TAN. Our research group has validated the *in-situ* electrochemical regeneration of commercial WAC resins as an effective technique for tandem regenerant production, resin regeneration, and nitrogen recovery. Although

ex-situ nitrogen recovery using NH₃-selective resins has been examined with commercial acids^{10,14}, *in-situ* analysis of NH₃-selective resins regenerated with electrochemically generated acids remains unexplored. More specifically, informed implementation requires exploration of how mild electrochemically generated acids protonate adsorbed ammonia while maintaining the zinc-carboxylate bond to minimize metal elution.

Nutrient recovery from NH₃-selective resins relies on maintaining the zinc-carboxylate bond during metal-ammine adsorption in wastewater and subsequent electrochemical regeneration. Bond breakage and zinc elution can occur due to outer-sphere competition with cations, inner-sphere competition from ligands, and protonation of the resin moieties under acidic conditions.^{10,14} Zinc elution limits the effectiveness of NH₃-selective resins by reducing the quantity of sites available for NH₃ adsorption. Furthermore, zinc elution can enhance effluent metal concentrations and thus pose environmental hazards, detrimental human health effects, and metal mitigation costs.^{15–17} A monovalent-selective membrane could prevent zinc transport and precipitation into the cathode chamber and allow for potential zinc reloading onto the resin. This membrane structure can prevent Zn²⁺ contamination of the aqueous ammonia product and maintain current efficiency within EC-IX systems. Systematically understanding operating conditions and system configurations is crucial for enhancing large-scale implementation of emerging nutrient recovery technologies.¹⁸ Therefore, conducting *in-situ* analysis on electrochemically regenerating NH₃-selective resins can advance their integration and feasibility in wastewater treatment.

The objective of this study was to investigate the electro-assisted regeneration of NH₃-selective resins in an EC-IX system, with the goal of understanding the tradeoffs between zinc elution and ammonia recovery. We investigated nutrient recovery across ammonia adsorption solutions and electrochemical regeneration in an EC-IX cell with anodic NH₃ protonation to NH₄⁺

and migration into an acidic cathodic chamber. Our main objectives were to: (1) determine how different ammonia adsorption conditions (pure ammonium solution, synthetic urine, and real urine) affect zinc elution and overall ammonia recovery, (2) examine the operating parameters (applied current, electrolyte composition, and TAN concentration) that maximize nutrient recovery while preventing zinc-carboxylate bond breakage, and (3) investigate the *in-situ* formation of zinc-carboxylate bonds to manage zinc elution. This proof-of-concept system enables exploration of three processes: selective ammonia adsorption, electrochemical regeneration, and nutrient recovery. Improved mechanistic understanding of how the solution environment and electrochemical parameters influence ammonium recovery and metal elution will advance nutrient separation and electrochemical recovery technologies and guide real-world implementation into wastewater treatment systems.

Materials and Methods

Aqueous Chemical Analysis

Cation concentrations (Na⁺, NH₄⁺, K⁺, and Zn²⁺) after adsorption and regeneration experiments were measured via ion chromatography on a Dionex ICS-6000 (IC, ThermoFisher/Dionex chromatograph, IonPac SCS1 column, unsuppressed, 4mM tartaric acid and 2 mM oxalic acid eluent, 1.0 mL/min, 30 °C). Unless the sample pH was already less than 3, samples were acidified with 2-5 μ L of 2 M H₂SO₄ to reach pH 3, where nearly all TAN was protonated (pH<<9.25 pK_a) and detectable on IC as NH₄⁺. Sample pH was measured with a pH meter (FP20, Mettler Toledo, Columbus, OH). Urine samples were collected and stored until full

hydrolysis occurred, defined as when urea concentration fell below the detection limit of 1 mg/L as measured spectrophotometrically (indophenol method)¹⁹ with a SEAL AA500 Segmented Flow Analyzer (SEAL Analytical Limited, Mequon, WI).

Ion Exchange Resin Metal Loading

We modified a macroporous hydrogen-form weak acid cation exchange resin (Dowex Mac 3, Sigma-Aldrich, St. Louis, MO) into a zinc-carboxylate resin to enhance ammonia selectivity using two-step ion exchange (from R-H⁺ to R-Na⁺ to R-Zn²⁺). 10,14 Zn²⁺ is an earth-abundant element that was chosen over other metals because it exhibited high selectivity towards NH₃ and intermediate binding affinity amenable to both NH₃ adsorption and regeneration. 20–22 We used a two-step exchange to accurately measure both Zn²⁺ uptake and Na⁺ removal with IC.

We placed 100 mL of neat hydrogen-form resin in 2 L of 1 M NaHCO₃ for 24 hours to completely exchange protons with Na⁺. As protons entered the solution, carbonic acid formed and rapidly decomposed in water to form H₂O and gaseous CO₂, which bubbled out of solution and thus increased solution pH.²³ We conducted this exchange for 24 hours until bubble formation ceased, indicating Na⁺ adsorption was complete.

Column experiments were used to modify sodium-loaded resins into zinc-loaded resins. 100 mL of sodium-loaded resin was placed into a cylindrical plastic column (200 mL volume, 1/4" inner diameter, 1' length, Spears Manufacturing, Sylmar, CA) and 6 L of 0.2 M ZnCl₂ solution was pumped at 3 mL/min for 72 hours using a peristaltic pump (Masterflex C/L, Vernon Hills, IL). Finally, we conducted batch adsorption with 1 L of 0.2 M ZnCl₂ solution for 24 hours to ensure complete Zn²⁺ loading. Resins were washed with nanopure water (resistivity 18.2 m Ω ·cm at 25

°C, Millipore Milli-Q System, Millipore Corporation, Billerica, MA) to remove any residual ZnCl₂ and the wash solution was tested on IC to ensure Na⁺ levels were below the detection limit of 3 nM.

Ammonia Loading

157

158

159

160

161

162

163

164

165

166

167

168

169

170

171

172

173

174

175

176

177

178

To elucidate the difference in ammonia selectivity in increasingly complex TANcontaining solutions, we used three adsorption solutions (full composition in **Table S1**): a pure ammonium solution containing 500 mM TAN (320 mM NH₃ as NH₄OH and 180 mM NH₄⁺ as NH₄Cl), a synthetic urine solution containing 230 mM TAN, and real hydrolyzed urine with 340 mM TAN. We began experiments with pure ammonium solution and synthetic urine because they are repeatable influents of known composition that establish proof-of-concept for electrochemical recovery of NH₃-selective adsorbents. Experiments with real urine, a more variable solution containing organic matter, used real wastewater to showcase nutrient recovery from realistic waste streams and explore how organic matter could affect adsorption mechanisms. All adsorption solutions besides the real urine were prepared with nanopure water and reagent-grade chemicals purchased from Sigma-Aldrich (St. Louis, MO). We collected real urine from consenting adults in the Shriram Center for Bioengineering and Chemical Engineering at Stanford University (Internal Review Board Protocol 60601). We first explored the effect of resin mass per solution volume on the ratio of ammonia adsorbed to zinc eluted, which compares the benefits of selective TAN recovery to the risks of adsorbent degradation. We used an isochoric process for the adsorption solution tests for the synthetic and hydrolyzed urine with 5 mL of solution and varying resin mass (10, 25, 50, 75, 100, 150, 200, 250, 500, 750, and 1000 mg resin/mL solution). Generally, we used 5 mL tubes for initial adsorption tests to minimize headspace and ammonia volatilization; because

higher resin masses required larger volumes, 750 and 1000 mg resin/mL adsorbate were conducted in 10 mL tubes. The ideal resin to solution ratio (i.e., resin dose) for a pure TAN solution (75 mg resin/mL solution) was chosen because our previous work indicated the ratio exhibited preferential TAN adsorption with minimal zinc elution (<1%). 14 Preliminary experiments showed that 8 hours was adequate for reaching equilibrium because the measured adsorption density was the same as for 24-hour experiments. Thus, we conducted 8-hour experiments and took 1-mL aliquots were taken for IC analysis and pH measurement.

Three metrics were used to evaluate resin performance: removal efficiency (% removal_A), adsorption density (q_f), and NH₃ adsorbed/Zn²⁺ eluted ratio.

Equation 1 defines the removal efficiency of each adsorbate in mmol/L (A = TAN, Zn²⁺, K⁺, or Na⁺). $C_{0,A}$ is the initial concentration and $C_{f,A}$ is the final concentration at equilibrium (adsorption after 8 hours).

191
$$\% \ removal = \left(\frac{C_{0,A} - C_{f,A}}{C_{0,A}}\right) * 100\%$$
 (1)

The adsorption density q_f (mmol adsorbate/g adsorbent) for each adsorbate A where V is the solution volume, and W is resin mass is defined by equation 2:

194
$$q_{f,A} = \frac{V(C_{0,A} - C_{f,A})}{W}$$
 (2)

The ammonia adsorbed to zinc eluted ratio was calculated by dividing the TAN percent adsorption by Zn^{2+} percent eluted in equation 3. $C_{TAN,f}$ and $C_{TAN,i}$ represent the final and initial aqueous TAN concentration during adsorption. V_{ads} is the volume of the adsorption solution while W is resin

mass. $C_{Zn}^{2+}{}_{f}$ is the final zinc concentration in aqueous solution. The initial zinc adsorption density, $q_{Zn}^{2}{}_{,i}$ was found by regenerating Zn-loaded resin in 0.5 M H₂SO₄ for 24 hours and analyzing the regenerant solution on IC.

$$\frac{Ammonia\ Adsorbed}{Zn\ Eluted} = \frac{\left(\frac{C_{TAN_i}V_{ads} - C_{TAN,f}V_{ads}}{C_{TAN,i}V_{ads}}\right)}{\left(\frac{C_{Zn^2+,f}V_{ads} - q_{Zn^2+,i}W}{q_{Zn^2+,i}W}\right)}$$
(3)

Electro-assisted Regeneration of NH₃-Selective Resin

We performed chronopotentiometry experiments to demonstrate that a proof-of-concept two-chamber EC-IX system could regenerate ammonia-saturated resins while minimizing zinc elution (**Figure 1a**). The anode was a titanium mesh coated with iridium mixed metal oxide (6 cm², Magneto Special Anodes, Netherlands) and the cathode was solid stainless steel (6 cm², 316 stainless steel, Small Parts, Plymouth, MI).^{11,13,24,25} The reactor was secured by two hollow Perspex plates ($10.2 \times 1.2 \times 5.3$ cm³) bolted between two solid Perspex plates ($10.1 \times 1.3 \times 8.7$ cm³) to create two 12-mL chambers. For all regeneration tests, 5 mL of ammonia-saturated resins were packed in the anode chamber of the EC-IX. This resin volume prevented direct contact with the anode and potential degradation from direct oxidation. Regeneration experiments were conducted in triplicate using the same batch of ammonia-saturated resin for reproducibility. Equation 4 defines the regeneration efficiency γ (%) where M_{ads} is moles of NH₃ adsorbed onto resin, and M_{anode} and $M_{cathode}$ are moles of TAN detected in each respective chamber.

$$\gamma_{regeneration} = \frac{M_{anode} + M_{cathode}}{M_{ads}} \times 100\%$$
 (4)

218

219

220

221

222

223

224

225

226

227

228

229

230

231

232

233

234

235

236

237

We classify regeneration as aqueous TAN in either analyte or catholyte while recovery describes aqueous TAN only in catholyte. We separately recirculated 100 mL of potassium solutions (K₂SO₄ for the analyte and KCl + 100 mM H₂SO₄ for the catholyte) at 40 mL/min with a peristaltic pump (Masterflex C/L, Vernon Hills, IL). Catholyte solutions for regeneration experiments contained 100 mM H₂SO₄ to prevent Zn(OH)₂ precipitation observed in preliminary experiments. We used a putatively monovalent-selective cation exchange membrane (CMS, Ameridia Inc., Napa, CA) to separate the analyte and catholyte chambers. Monovalent-selective membranes use size exclusion to block divalent ions from transporting through the membrane matrix. 26-28 K⁺ was chosen as the electrolyte cation because it exhibits sufficient peak separation with NH₄⁺ for reproducible IC measurements. Sulfate was chosen due to its abundance in the environment and stability in anodic conditions, while chloride was chosen due to its environmental abundance and stability in cathodic conditions.^{29,30} Anolyte and catholyte concentrations were always matched (both 10 mM or both 100 mM) to examine concentration effects on regeneration efficiency and energy consumption. Zinc eluted during regeneration was recorded during each sampling point. To examine the influence of OER on EC-IX performance, we applied two current densities (0.08 mA/cm² and 4.96 mA/cm²) for 6-hour experiments using a potentiostat (Reference 3000, Gamry, Warminster, PA). These current densities were anticipated to facilitate electromigration of cations (Equation S1), allow regeneration via protons from OER (i.e., water oxidation), and minimize extreme pH drops that promote metal elution. ^{13,31} The two current densities used allowed interrogation of the relative effects of diffusion and electromigration on ammonium transport in the EC-IX system. Specifically, the 0.08 mA/cm² case showed 80% migration due to electromigration

and 20% due to diffusion; the 4.96 mA/cm² showed 90% migration due to electromigration and 10% to diffusion.

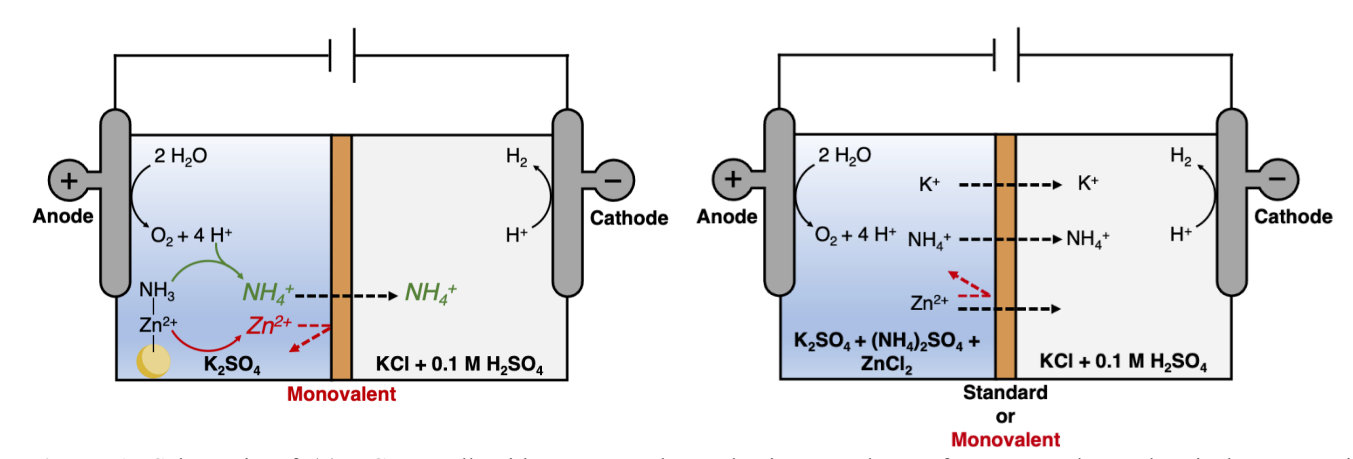


Figure 1: Schematic of (a) EC-IX cell with a monovalent-selective membrane for *in-situ* electrochemical regeneration experiments and (b) electrolysis cell to explore cationic transport across a standard cation exchange membrane and a monovalent-selective membrane. The electrochemical cell produces acid in the anolyte through OER and base in the catholyte through HER. Dotted arrows illustrate movement across each membrane during electrolysis. The monovalent-selective membrane retains zinc in the anode chamber and ammonium in the cathode chamber for recovery. The standard membrane allows for all cation to transport from anode chamber to cathode chamber.

Adsorbent Characterization

238

239

240

241

242

243

244

245

246

247

248

249

We used Fourier-transform infrared spectroscopy (FTIR) to examine the pre- and postelectrochemical regeneration bonding environment of NH₃-selective resins with a Nicolet iS50 ATR FT/IR Spectrometer (HeNe laser, Thermo Nicolet Company, USA). The wavenumber range of FTIR spectra was 2000 cm⁻¹ to 800 cm⁻¹. To ensure homogeneity, all samples were ground with a mortar and pestle before FTIR analysis.

Ionic Transport through Two-Chamber Electrolysis Cell

Although we aimed to avoid zinc elution from the resins, its elution and transport could affect ammonia recovery by influencing the transference number (i.e., the fraction of the total

current carried by each ionic species). To investigate the consequences of potential zinc elution, we explored the cationic transport of Zn²⁺ against other relevant cations in a two-chamber electrolysis cell without resin (**Figure 1b**). The anode and cathode chambers were separated by two types of cation exchange membrane (CEM). These membranes are categorized as either a standard membrane (CEM, CMI-7000, Membranes International Inc., Ringwood, NJ) or monovalent-selective membrane (CMS, same as used for electrochemical regeneration with resin) for further reference. More information on membrane properties is listed in **Table S2**.³²

We evaluated three solutions with varying concentrations of Zn^{2+} , NH_4^+ , and K^+ to compare the transference number of each compound. These solutions were chosen to elucidate the effect of the TAN/Zn^{2+} ratio (2:1, 1:1, 0:1) on cation transference numbers (**Table S3**). Equation 5 shows the transference ratio (δ) for ions x and y where t_i is the transference number, Z_i is the ion valence (+1 for monovalent cations and -1 for monovalent anions), C_i is ion concentration in the cathode chamber, and λ_i is equivalent ionic conductivity in the aqueous phase.

$$\delta = \frac{t_x}{t_y} = \frac{|Z_x|C_x\lambda_x}{|Z_y|C_y\lambda_y} \tag{5}$$

We conducted experiments using a BioLogic potentiostat (VMP-300, BioLogic Sciences Instruments, Grenoble, France) with the standard and monovalent-selective membrane at a current of 4.96 mA/cm², enabling electromigration through the cation exchange membrane and mild acid production via electrochemical water electrolysis.^{33,34}

*In-situ Formation of Zn*²⁺- *RCOO*⁻ *bond*

To demonstrate in-situ reformation of the zinc-carboxylate bond, flow-through experiments were performed in a two-chamber electrochemical reactor (Figure S2). We regenerated NH₃-selective adsorbents at the high current density and electrolyte condition (100 mM and 4.96 mA/cm²) and recorded the final NH₃ regeneration efficiency and Zn²⁺ elution along with initial adsorption densities. Subsequently, the same resin was placed in the anode chamber to facilitate in-situ reformation within the same two-chamber EC-IX cell used for electrochemical regeneration and ionic transport experiments. Anolyte and catholyte chambers each contained 100 mL of electrolyte, with the bottles initially filled with nanopure water. We pumped 2 L of 50 mM ZnCl₂ into the anolyte bottle at 35 mL/min to supply Zn(II) ions into the system. Electrolyte solutions were recirculated with a separate pump at 40 mL/min. Recovery flow rates ensured 100 mL recirculation in electrolyte bottles and differed between the two pumps due to a difference in tubing diameter (1/16" for EC-IX recirculation and 1/12" for ZnCl₂ flow). The analyte outflow was placed in a waste bottle to prevent the recirculation of NH₃ and promote Zn²⁺ ion exchange with the carboxylate sites. We collected 1 mL samples from the analyte (holding bottle and outflow) and catholyte at several time points over the 2-hour experiment. Afterwards, the reloaded resin was placed in hydrolyzed urine for another adsorption stage at the 100 mg resin/mL (as opposed to 75 mg/mL for pure ammonium) solution ratio for 24 hours. Finally, the resin was regenerated with 5 mL of 0.5 M H₂SO₄ and analyzed by IC to determine the final ammonia and zinc adsorption densities and to evaluate in situ reformation.

288

289

269

270

271

272

273

274

275

276

277

278

279

280

281

282

283

284

285

286

287

Results and Discussion

Effect of Dosage and Ammonia Selectivity during Metal-Ammonia Adsorption

290

291

292

293

294

295

296

297

298

299

300

301

302

303

304

305

306

307

308

309

310

311

Effective ammonium recovery with metal-ligand adsorbents relies on maximizing NH₃ adsorption and preserving the zinc-carboxylate bond. Solution composition, particularly pH and TAN concentration, profoundly impacts the stability of metal-ligand adsorbents. Based on previous work, the optimal pH for ammonia adsorption onto NH₃-selective adsorbents is 9-10 and the optimal TAN concentration is 200-300 mequiv N/L.¹⁰ These optimal solution conditions make hydrolyzed urine (pH 9.2, 300-500 mequiv N/L) a promising adsorption solution. However, three challenges for ammonia recovery occur outside of optimal conditions: (1) outer-sphere electrostatic interactions between the carboxylate functional group on WAC and competing cations in solution, (2) inner-sphere (ligand binding with Zn²⁺) interactions in solutions with high TAN concentrations, and (3) protonation of carboxylate moieties in acidic conditions^{10,14} (**Figure S3**). We first studied the mass to solution ratio for synthetic and hydrolyzed urine and its impact on cation adsorption, metal elution, and the solution pH 9. At higher resin mass to solution ratios (i.e., resin doses), TAN adsorption plateaued due to excess adsorption sites binding to all available NH₃ in solution (Figure 2a). Because NH₃ is a weak base, its adsorption acidifies the solution phase and pushes the NH₃/NH₄⁺ towards NH₄+, which exhibits lower affinity for the adsorbent than NH₃. This self-limiting phenomenon has been validated in multiple studies of Zn-loaded NH₃ adsorbents; adding buffer to keep pH above 9.25 successfully enhanced adsorption efficiency.^{5,14} The high buffering capacity of real urine likely plays a similar role due to higher total ammonia and total carbonate concentrations than in synthetic urine (**Table S1**).

At higher resin doses, the adsorption solution pH deviates from the optimal pH range (9-10) for selective adsorption due to shifts in equilibrium between ligand bond and solution

environment^{10,14} (**Figure 2b**). Because NH₃ interacts with the Zn²⁺ ligand and NH₄⁺ does not, NH₃ can uniquely be removed via ligand binding.^{20,21} Adsorption decreases the conjugate base (NH₃) concentration and increases the conjugate acid (NH₄⁺) concentration, which decreases the solution pH. The natural buffering capacity of human urine³⁵ (predominantly by carbonate and ammonia species) likely mitigated sharp pH drops and increased TAN adsorption at lower resin to solution ratios in real urine compared to synthetic urine. For real urine, bicarbonate (pKa HCO₃⁻/CO₃²-=10.3) are present at concentrations of 31-32.2 mmol/L.^{11,19,36} For synthetic urine in this study, the total carbonate concentration was lower at 23.6 mmol/L. The continued pH decline after the plateau in TAN adsorption was likely due to increased zinc binding to water/hydroxide ligands and releasing H⁺ after metal elution.³⁷ The change in solution environment also altered the ideal ammonia adsorbed to zinc elution ratio (Figure 2c). We observed ideal ratios of 50 and 100 mg resin/mL of solution for 230 mM TAN synthetic urine and 340 mM TAN real urine, respectively. At lower resin mass to solution doses, selective TAN removal resulted in minimal zinc elution, while at higher doses, improved TAN removal led to other cations outcompeting Zn²⁺ and electrostatically interacting with the carboxylate functional group.

312

313

314

315

316

317

318

319

320

321

322

323

324

325

326

327

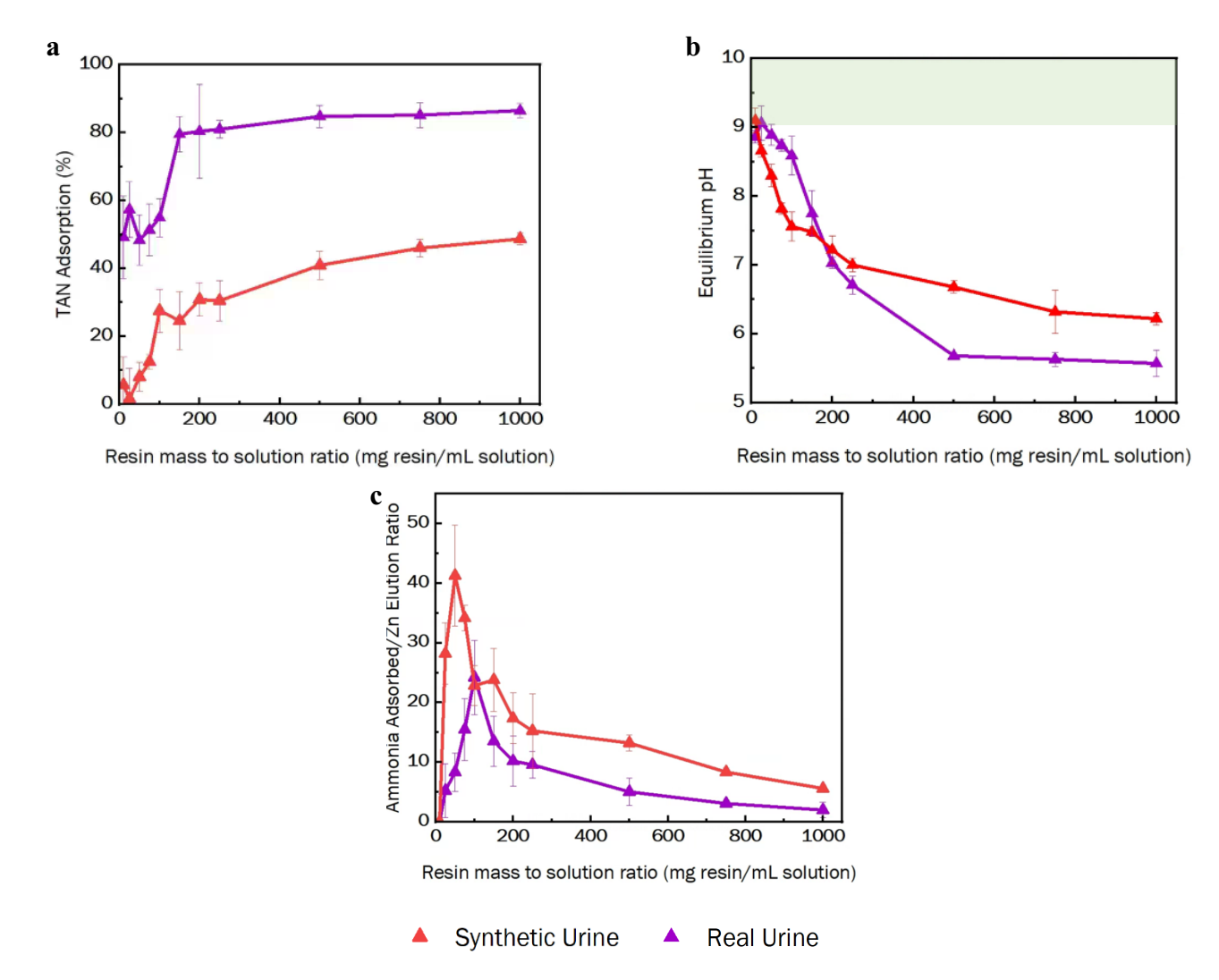


Figure 2: A comparison of real hydrolyzed and synthetic urine across a range of resin doses exploring (a) TAN adsorption efficiency (b) pH of the equilibrium solution with optimal pH shaded in green and (c) ratio of ammonia adsorbed to zinc eluted. Error bars not shown are smaller than symbols.

In-situ Electrochemical Regeneration

The electrochemical regeneration efficiency of NH₃-selective adsorbents determines TAN recovery. More specifically, electrochemical operating parameters can tune electrolyte pH and facilitate protonation of removed ammonia into recovered ammonium. Both the molar

concentration of electrolyte solution and applied current influence the rate of water electrolysis and thus the bulk solution pH. 34,38-40 We compared two analyte concentrations (K₂SO₄ at 10 mM and 100 mM) and two current densities (0.08 mA/cm² and 4.96 mA/cm²) using the monovalentselective membrane. Across the regeneration experiments with resin that treated real urine, NH₄⁺ regeneration efficiency from electrochemical regeneration was between 60-90% (Figure 3). Using 100 mM electrolyte produced high total ammonia regeneration across both applied current densities (83% vs 94% for 0.08 mA/cm² and 4.96 mA/cm², respectively) (Figure 3a). A twosample t-test revealed that the two mean NH₄⁺ regeneration values for 0.08 mA/cm² and 4.96 mA/cm² after 6 hours are not statistically different (p-value of 0.143). However, a two-sample ttest showed that the two mean NH₄⁺ regeneration values for 10 mM K₂SO₄ and 100 mM K₂SO₄ after 6 hours are statistically significant (p-value of 0.0113). For constant applied current density, the difference in electrolyte molar concentration varied the total ammonia regeneration more (61% vs 83% for 10 mM and 100 mM, respectively) (Figure 3b). Overall, increasing the molar concentration and current density resulted in a lower final solution pH, which increased the protonation of ammonia to ammonium, thereby enhancing recovery into the cathode and facilitating simultaneous regeneration of the zinc-carboxylate bond (**Table S4**).

334

335

336

337

338

339

340

341

342

343

344

345

346

347

348

349

350

351

352

353

354

355

356

We examined the distribution of NH₄⁺ across both chambers and detected the lowest recovery into the cathode chamber in 10 mM K₂SO₄ at 0.08 mA/cm² (63% regeneration but only 21% recovery in cathode chamber) (**Figure S4a**). This recovery was likely due to the low electrochemical potential difference across the membrane hindering cation transport.^{41,42} In contrast, the concentrated 100 mM K₂SO₄ electrolyte exhibited higher total ammonia regeneration across both applied current densities (83% total regeneration and 34% recovery in cathode for 0.08 mA/cm² vs 94% total regeneration and 48% recovery in cathode for 4.96 mA/cm²) (**Figure S5a**

and Figure S6a). In every instance, the overall ammonium recovery to the cathode remained below 50%. However, like the total ammonia regeneration, recovery varied directly with molar concentration and applied current density. Ammonia recovery was lower in our experiments compared to previous nutrient recovery technologies because of the low applied current density (approximately 0.08 and 4.96 mA/cm² in this study; 30-180 mA/cm² for electro-assisted regeneration of urine-loaded commercial cation exchange resins¹³; 3-10 mA/cm² for electrochemical stripping^{25,43}). Because we were interested in identifying the impact of operating parameters more than maximizing performance in this study, lower ammonia recovery was not a concern. Ultimately, too low of a current density would hinder ammonium electromigration and favor H⁺ transport due to their higher ionic mobility.⁴⁴ To emphasize the regeneration and recovery of ammonium from NH₃-selective adsorbents at these conditions, the applied current in the electrochemical system should be higher than 0.08 mA/cm². Based on the electrochemical regeneration results, the electrolyte concentration was the most influential operating parameter that dictates ammonium regeneration.

We complemented the NH₄⁺ migration analysis by examining the competing cation in the electrolytes, K⁺. Because we measured aqueous K⁺ concentrations in the anolyte and catholyte, any K⁺ trapped in the membrane would not have been included in our measurements. During the 10 mM at 0.08 mA/cm² scenario, we identified that summing anode and cathode chamber concentrations left 17% of K⁺ unaccounted (**Figure S4b**). Increasing the background ion concentration to 100 mM improved the transfer of K⁺ from anode to cathode and led to lower unaccounted K⁺ fractions (6% for 0.08 mA/cm², 4% for 4.96 mA/cm²) (**Figure S5b** and **Figure S6b**). The low applied current likely led to K⁺ sorption in the membrane or the resin rather than transport, which we did not distinguish. The same phenomena could occur for NH₄⁺, meaning the

"remaining" fraction contains both membrane and resin sorption. Ion sorption in cation exchange membranes is enhanced at low applied current density because of low cation flux across the membrane. Compared to K⁺, unaccounted NH₄⁺ generally exceeded the background electrolyte in all electrochemical regeneration cases at each sample point (Figures S4-S6). While K⁺ and NH₄⁺ sorption were prevalent in 10 mM K₂SO₄ at 0.08 mA/cm², operating at higher applied current density mitigated ion sorption and facilitated ion transport due to a stronger electromigration driving force. Ion sorption was the main sorption mechanism and the unaccounted K⁺ was reversed after acid regeneration (0.5 M of H₂SO₄ at pH 0.45) closed the mass balance (Figure S7a). As an alternative to acid regeneration, saturating cation exchange resins with nanopure water after electrochemical regeneration could remove the lingering cations from fixed charged groups in the membrane. In the membrane of the same property of

Closing the mass balance of NH₄⁺ required additional chemical regeneration with strong acids (0.5 M of H₂SO₄ at pH 0.45) after electrochemical regeneration of ammonia-saturated resin (**Figure S7b**). As highlighted earlier, we observed the highest regeneration efficiency in the 100 mM K₂SO₄ at 4.96 mA/cm² and the lowest in the 10 mM K₂SO₄ at 0.08 mA/cm² condition. Nevertheless, most resin sites were regenerated across all experimental conditions and facilitated ammonium regeneration from ammonia-saturated resin. At higher K₂SO₄ concentration and applied current density, the final solution pH trended acidic (**Table S4**). Dynamic bias systems, where regeneration occurs at 0.08 mA/cm² and recovery occurs at 4.96 mA/cm², could circumvent the zinc elution and ion sorption challenges.



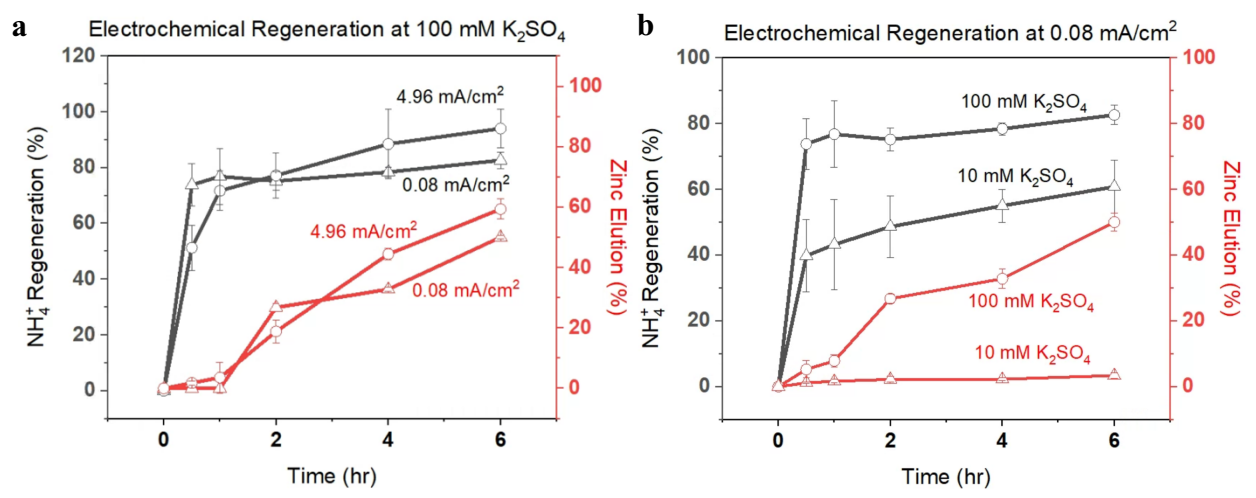


Figure 3: Total ammonium regeneration (left axis) and zinc elution (right axis) under experimental conditions: (a) 100 mM with varied applied current density and (b) 0.08 mA/cm² with varying electrolyte molar concentration. Error bars not shown are smaller than symbols.

Zinc Elution

Across all experimental conditions, we detected zinc elution in the anode chamber after 1 hour of operation. For zinc elution from ammonia-saturated resins, the combination of low current and low K^+ concentration led to minimal zinc elution (<4%) by the end of the experiment (**Figure 3b**). Experiments with higher K^+ electrolyte concentrations enhanced K^+ competition with Zn^{2+} for carboxylate moieties. Furthermore, the concentrated anolyte salt (100 mM) led to a more drastic pH drop (**Table S4**). In the 10 mM at 0.08 mA/cm² case, the initial pH was 5.5 ± 0.5 and final pH was 4.2 ± 0.6 ; in the 100 mM at 0.08 mA/cm² case, the initial pH was 5.3 ± 0.2 and final pH was 3.3 ± 0.1 . Similar to regeneration efficiency, the anolyte concentration influenced zinc elution more than applied current density. The final solution pH also directly correlated with the stability of zinc-carboxylate bonds with more acidic conditions leading to more zinc elution. The choice of electrolyte could improve zinc-carboxylate stability during regeneration by limiting the OER

overpotential on iridium oxide anodes. For example, sodium ions exhibit a smaller overpotential enhancement of OER compared to potassium ions.⁴⁸ Furthermore, innovative resin chemistries that strengthen the zinc-carboxylate bond could also improve ammonia adsorption in complex wastewaters and advance electrochemical ammonium recovery technologies.⁵ Finally, combining pH buffer resins (tertiary amine) with NH₃-selective resins¹⁴ could also mitigate pH drops and exhibit tandem improvements of ammonium regeneration efficiency and mitigation zinc elution across electrochemical operating parameters.

Adsorbent Characterization

Ideal electrochemical regeneration protonates NH₃ to NH₄⁺ while preserving the zinc-carboxylate bond. Identifying changes in the ligand structure between pre- and post-regeneration adsorbents will help inform how experimental conditions (i.e., adsorption solution, electrochemical operating parameters) influence ammonia binding and zinc elution. Urine-loaded adsorbents exhibited similar absorbance peak intensity with post-regenerated adsorbents at 0.08 mA/cm² compared to less pronounced peak intensity in the 4.96 mA/cm² experiments (**Figure 4**). Peaks across all experimental conditions match antisymmetric (1537 cm⁻¹) and symmetric (1407 cm⁻¹) stretches for carboxylate functional groups.⁴⁹ Electrochemical regeneration at 0.08 mA/cm² did not remove all NH₃ from ligand binding and a mild N-H bend exists between 950 cm⁻¹ to 1120 cm⁻¹. Examining all regeneration conditions with the real urine-loaded resin, the subtle C=O stretch at 1700 cm⁻¹ is likely caused by the protonation of carboxylate sites to carboxylic acid. Furthermore, the transition from the COO⁻ asymmetric stretch to the C=O stretch is less

pronounced in the 100 mM at 4.96 mA/cm² concentration experiment where zinc elution prevailed during regeneration. A strong C=O peak at the 1700 cm⁻¹ is observed on the neat WAC-H⁺ spectra due to preservation of the proton bond.⁵⁰ The C=O stretch is prevalent across all electrochemical regeneration experiments regardless of adsorption solution or electrochemical operating parameters (**Figure 4, Figure S8).** Comparing spectra across ammonia adsorption solutions, pure ammonium TAN and synthetic urine produced similar intensity peaks during electrochemical regeneration at 100 mM at 4.96 mA/cm² compared to adsorbents before regeneration (**Figure S8**). Based on these results, additional adsorption and regeneration cycles could be performed after electrochemical regeneration of NH₃-selective adsorbents.

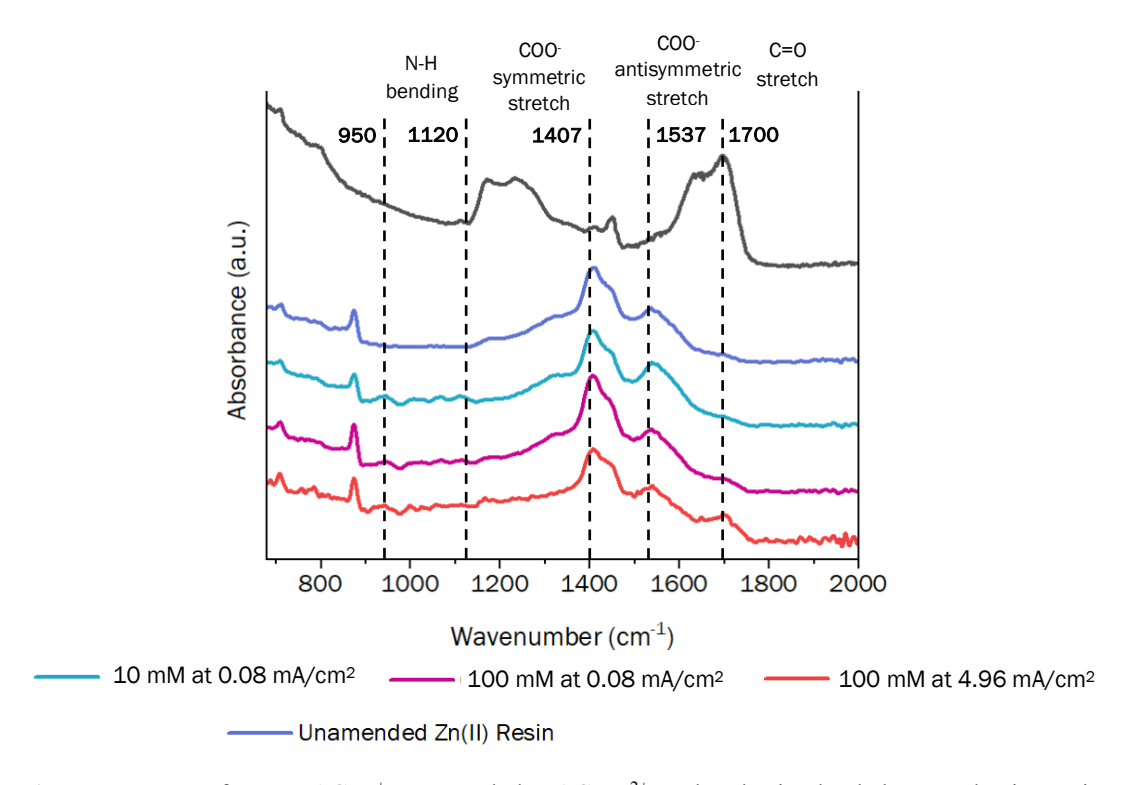


Figure 4: FTIR spectra of neat WAC-H⁺, unamended WAC-Zn²⁺, and real urine loaded NH₃-selective resins after electrochemical regeneration under different conditions.

Ion Migration: Transference of Ammonium, Potassium, and Zinc

To examine how eluted zinc influences cation transport, we investigated the transference number of relevant cations (K⁺, NH₄⁺, and Zn²⁺) in several electrolytes (compositions in **Table S3**) across standard and monovalent-selective cation exchange membranes. K⁺ and Zn²⁺ can compete with NH₄⁺ for transport across membranes and diminish NH₄⁺ recovery in the catholyte.⁵¹ In both membranes, the transference number for all cations (K⁺, NH₄⁺, and Zn²⁺) peaked within the first 30 minutes and gradually decreased during the experiment (**Figure 5**). Compared to the standard membrane, the monovalent-selective membrane exhibited less relative K⁺ transport and more relative NH₄⁺ transport. For the standard membrane, K⁺ and NH₄⁺ contributed most of the charge transport throughout the experiment (**Figure 5a**). Due to its larger ionic radius, Zn²⁺ contributed the least amount of charge, migrating slower through membrane matrix than monovalent ions with smaller ionic radii (K⁺ and NH₄⁺).⁵²

For the monovalent-selective membrane, a similar transference number trend was observed, where the membrane completely hindered the migration of Zn²⁺ ions into the cathode chamber due to size exclusion, leaving only K⁺ and NH₄⁺ transport (**Figure 5b**). These results indicate that implementing a monovalent-selective membrane would not hinder the total charge carried nor ammonium recovery during electrochemical regeneration of NH₃-selective resins since H⁺ would supplement lost charge. For both membranes, as the transference number of cations decreased from migration there was a gradual increase in current carried from protons produced by OER. To maintain a constant current, proton transport increased due to cation depletion within the system, with proton production from OER supplementing charge during the later stage as

cations migrated from anode to cathode.¹³ During *in-situ* regeneration of NH₃-selective resins, we expect the concentrations of the summed concentration NH₄⁺ and Zn²⁺ will be lower compared to that of K⁺ (background electrolyte).

468

469

470

471

472

473

474

475

476

477

478

479

480

481

482

483

484

485

486

487

488

489

As we changed the concentration, we noticed a preservation in trends across membranes but observed differences in transference from each non-H⁺ cation (Figure 5 vs Figure S9). The reduced ionic conductivity of the monovalent-selective membrane compared to the standard membrane decreased the NH₄⁺ transference, thereby lowering the overall transference contribution from non-H⁺ cations. In the standard membrane, the higher mobility and abundance of K⁺ cations compensated for the lower charge carried by Zn²⁺ to ensure a constant current was maintained in the system. Compared to the equimolar case, lower initial NH₄⁺ concentration led to more charge carried by K⁺ for both the standard and monovalent-selective membrane (92% and 42% at 0.5 hours, respectively) (**Figure S9**). However, similarly to the equimolar condition, proton generation from OER supplemented most of the charge at longer electrolysis times. When we reduced the ionic strength of the electrolyte by removing NH₄⁺ but maintained equal concentrations of K⁺ and Zn²⁺, K⁺ was the dominant charge carrier. (**Figure S10**). However, when NH₄⁺ was present in solution then H⁺ was the predominant charge carrier in both membranes (**Figure 5** and **Figure S9**). Compared to the monovalent-selective membrane, where the transference number of Zn²⁺ was hindered due to size ∂n exclusion, in the standard membrane, the slow migration of Zn²⁺ led to a low transference number (Figure S11). Across all ion migration experiments, slower Zn²⁺ diffusion across the standard and monovalent-selective membrane forced the competing monovalent cations (i.e., K⁺ and NH₄⁺) to carry the charge until OER produced sufficient protons for migration.

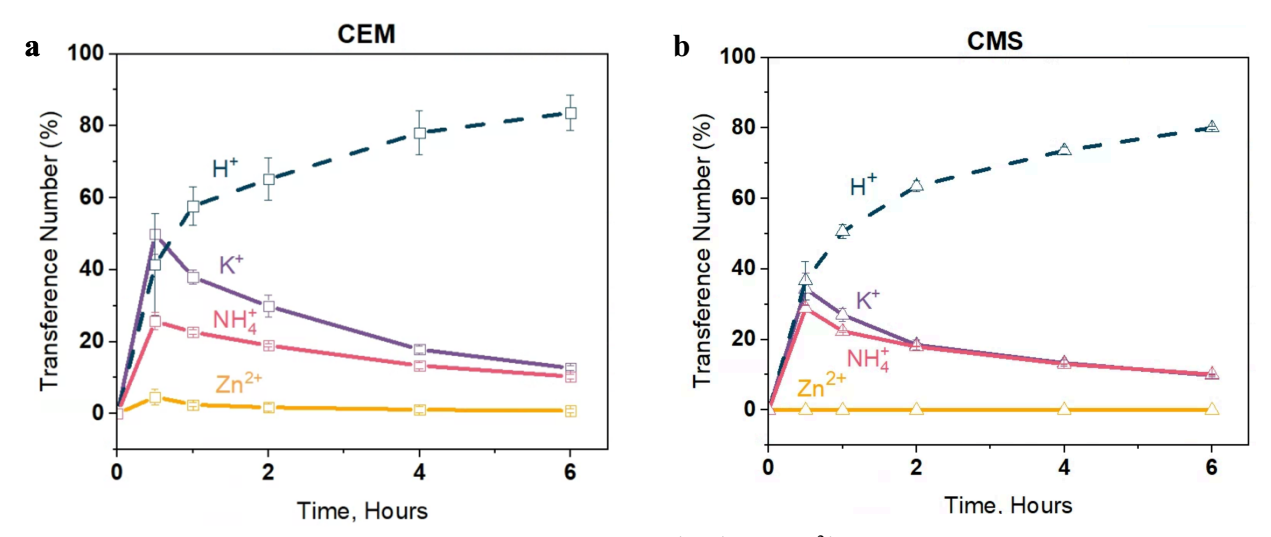


Figure 5: Comparison of total transference numbers of NH₄⁺, K⁺, and Zn²⁺ during equimolar (10 mM) cationic migration experiments conducted at 4.96 mA/cm² across (a) standard (CEM) and (b) monovalent-selective (CMS) membrane. Solid lines represent calculations based on measured ion concentrations, while the dashed line for protons was determined using the remaining current balance. Error bars not shown are smaller than symbols.

Transference Ratio

To further evaluate cation migration across each membrane, we calculated the ratio of transference numbers (transference ratio) of NH_4^+ ions compared to the background electrolyte cation, K^+ . For the monovalent-selective membrane at equimolar concentration (10 mM $K^+/NH_4^+/Zn^{2+}$), the transference ratio between K^+ and NH_4^+ hovered near 1, indicating equal migration of both cations from anode to cathode chamber (**Figure 6a**). Compared to the standard membrane, the transference ratio was enhanced in the monovalent membrane (1.05 \pm 0.01 at 6 hours for the monovalent and 0.73 \pm 0.14 standard membrane). The standard membrane's lower NH_4^+ migration to the catholyte was likely due to Zn^{2+} binding in the standard cation exchange

membrane, which could block exchange sites and limit the migration for cations with smaller hydration shells (i.e., K^+ and NH_4^+). 52,53

Based on the transference ratio in the monovalent-selective membrane, the rejection of Zn^{2+} did not hinder cation migration of K^+ or NH_4^+ nor charge carried within the system. Due to similar ionic size and charge^{5,8}, the transference ratio of K^+ and NH_4^+ was governed by the initial ionic ratio between the cations. When we lowered the initial concentration of NH_4^+ , the resulting NH_4^+/K^+ transference ratio (~0.5 NH_4^+/K^+) in both membranes followed the initial ionic ratio in the electrolyte (**Figure 6**). Overall, these experiments without resin show that using a monovalent-selective membrane could prevent metal precipitation in electrochemical recovery systems, enhance ammonium recovery (ion migration of NH_4^+), and avoid adverse effects on OER.

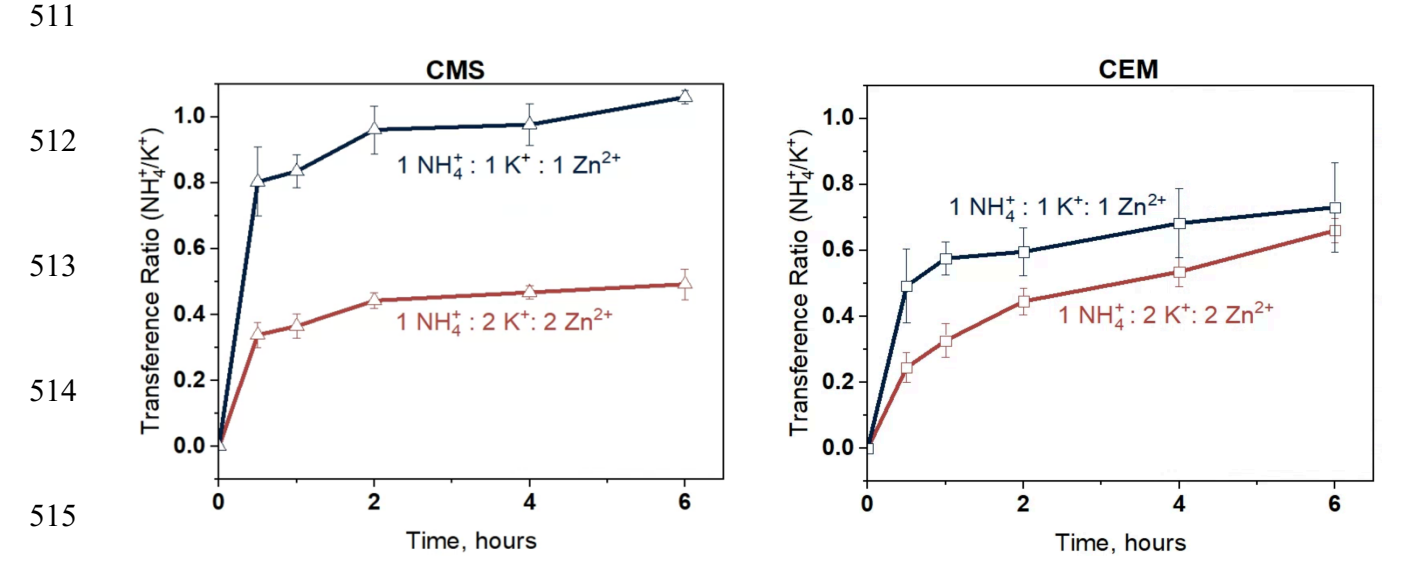


Figure 6: The transference ratio of NH_4^+/K^+ during cationic migration experiments conducted at 4.96 mA/cm² across (a) monovalent-selective (CMS) and (b) standard (CEM) membrane. Blue line indicates the equimolar (10 mM of K^+ , NH_4^+ , and Zn^{2+}) condition while red indicates the decreased ammonium condition (10 mM of K^+ and Zn^{2+} ; 5 mM of NH_4^+)

520

521

522

523

524

525

526

527

528

529

530

531

532

533

534

535

536

537

538

In-situ Zinc Recovery and Cyclic Ammonia Adsorption

Electrochemical regeneration of ammonia-saturated resins facilitated ammonia protonation and zinc elution to varying degrees across experimental conditions. We applied our insights from ex-situ zinc-carboxylate column loading and ligand exchange chemistry to evaluate in-situ reformation of the zinc-carboxylate bond after regeneration. *In-situ* reformation achieved similar adsorption densities for Zn^{2+} (7.27 \pm 0.47 mmol of Zn^{2+}/g resin and 6.29 \pm 0.72 mmol of Zn^{2+}/g resin for urine adsorption cycles 1 and 2, respectively) and NH₃ (3.8 \pm 0.63 mmol of NH₃/g resin and 3.2 ± 1.3 mmol of NH₃/g resin for hydrolyzed urine adsorption cycles 1 and 2, respectively) (**Figure 7**). Maximum Zn²⁺ elution across experimental parameters was 5.8 mmol of Zn²⁺/g resin (i.e., 4.34 mg Zn²⁺/L), which is below the EPA Zn²⁺ discharge limit of 5 mg/L.⁵⁴ A two-sample ttest revealed that the two means for NH₃ and Zn²⁺ are not statistically different (p-value of 0.12 for NH₃ and 0.17 for Zn²⁺). The pH of the 50 mM ZnCl₂ solution (~6.2) helped maintain the WAC functional group speciation towards carboxylate instead of carboxylic acid. Simultaneously, ion exchange was aided by NH₃ removal likely from increased zinc-ammine complexes in solution. 10,55,56 We further explored zinc-carboxylate bond reformation with Na⁺ loaded resins and >95% of sites were zinc-loaded after 180 minutes (Figure S12). Our results indicate in-situ reloading procedures could facilitate long-term selective resin use for ammonium recovery. A semicontinuous electrochemical treatment system that combines continuous flow for zinc loading and batch for ammonia adsorption could promote full-scale ammonium recovery technologies.⁵⁷

Based on these results, *in-situ* reformation of the zinc-carboxylate bond can be achieved without applied current and with minimal chemical inputs. We encourage future research efforts to continue exploring metal-ligand coordination chemistry and adsorbent stability to promote ammonium recovery from waste streams.

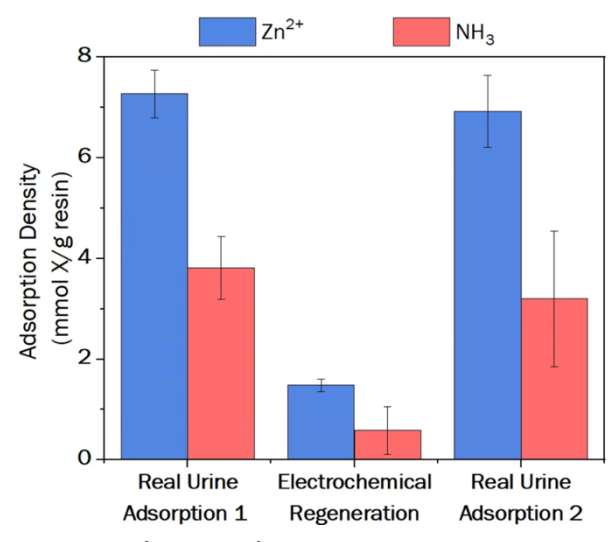


Figure 7: The adsorption density of Zn²⁺ and NH³ on NH₃-selective resin. 'Real Urine Adsorption 1' indicates adsorption density after urine adsorption with 340 mM TAN prior to regeneration. 'Electrochemical Regeneration' indicates the adsorption density after regeneration at 100 mM and 4.96 mA/cm². 'Real Urine Adsorption 2' shows the final adsorption density after in-situ reloading with 50 mM ZnCl₂ and then 340 mM TAN and urine loading with 340 mM TAN.

Conclusion

This study explored the ammonia adsorption efficiency (ammonia removal) and the *in-situ* electrochemical regeneration (ammonium recovery) of NH₃-selective adsorbents to advance ion exchange technologies in water treatment and circular nitrogen management. We aimed to understand the effect of *in-situ* electrochemical regeneration and validate a proof-of-concept system rather than optimize NH₃-selective adsorbents in electrochemical systems. Zinc elution

from the carboxylate moiety limits the effectiveness of NH₃-selective adsorbents for ammonia removal by sacrificing the adsorption sites. By exploiting a zinc elution pathway (inner-sphere ligand bonding), we reformed the bond *in*-situ which can enable continuous TAN recovery after multiple adsorption and regeneration cycles. We explored the resin characterization and process performance across aqueous ammonia solution of varying complexity (pure ammonium, synthetic urine, and real urine with organics) and electrochemical regeneration with varying current density and electrolyte concentrations. Electrolyte concentration impacted ammonium regeneration efficiency more than current density, and the most extreme conditions exhibited >97% ammonium regeneration efficiency. However, a tradeoff exists between ammonia recovery and zinc elution that could hinder implementation. Using a monovalent-selective membrane, we minimized potential Zn²⁺ discharge to the environment and maintained a pure recovered TAN product. Flowthrough experiments showed that aqueous Zn²⁺ removed ammonia from carboxylate moieties. The preservation of the carboxylate chemistry after regeneration highlights the potential for multiple adsorption-regeneration cycles, as supported by FTIR resin characterization that evinced minimal changes in bonding environment of electrochemically regenerated resin compared to unamended NH₃-selective adsorbents.

551

552

553

554

555

556

557

558

559

560

561

562

563

564

565

566

567

568

569

570

571

572

573

Electrochemically mediated regeneration of TAN-selective adsorbents furthers the integration of adsorbents and electrochemistry to advance selective nitrogen separations. Using ligand exchange for improved ammonia removal followed by electrochemical regeneration for ammonia recovery overcomes the selectivity and regeneration challenges of existing adsorptive nitrogen recovery techniques. We identified a tradeoff between ammonium regeneration and zinc eluted within electrochemical systems. To preserve the zinc-carboxylate bond while facilitating adequate ammonium recovery, electrochemical operators should use low molar concentrations (10

mM K₂SO₄) and applied current (0.08 mA/cm²) to minimize zinc elution (4%) and maximize NH₄⁺ regeneration (61%). With 100 mM K₂SO₄ and 4.96 mA/cm² we increased the ammonium regeneration efficiency to >97% but observed 60% zinc elution. Although we pursued proof-ofconcept and mechanistic understanding over process optimization, we achieved an overall N recovery of 39%, which was limited by low N transfer between chambers (48%). We summarize the N removal and recovery at each stage, highlight suggested improvements, and compare to established analogous technologies (Table S5). Ultimately, we demonstrate the improved selectivity and recovery of TAN at low concentrations with NH₃-selective adsorbents and implore further exploration in complex wastewaters with varying TAN concentrations (e.g., 0.1-10 mg TAN/L in fertilizer runoff^{59,60}, 41-50 mg TAN/L in municipal wastewater influent^{61,62}, and 30-2500 mg TAN/L in industrial wastewaters).⁵⁸ Future work will further interrogate multi-cycle adsorbent durability using X-ray absorption spectroscopy (X-ray absorption near edge structure and extended X-ray absorption fine structure) to identify the coordination environment and elemental distribution of Zn²⁺ on ammonia-loaded and electrochemically regenerated resin. Furthermore, conducting column experiments can significantly enhance the understanding of resin stability during NH₃ adsorption and electrochemical regeneration. Column experiments will help inform process mechanisms and advance nutrient recovery technologies that align with practitioners. Tracking the stability of the ammonia-zinc complex in adsorption, electrochemical regenerate, and reformation solutions will enable electrochemical separations for nitrogen removal and recovery. By tuning the electrochemical operating parameters and establishing process performance metrics for effective TAN recovery and ligand stability, this study advances selective ammonium recovery technologies, promotes a circular nitrogen economy, and repurposes waste into a value-added product.

574

575

576

577

578

579

580

581

582

583

584

585

586

587

588

589

590

591

592

593

594

595

596

Acknowledgements

Funding for this work was made possible by the Department of Chemical Engineering at Stanford University and a P3 (People, Prosperity, and the Planet) award from the U.S. Environmental Protection Agency. E.A. was supported through the National Science Foundation Graduate Research Fellowship (Grant No. 1656518). C.M.L. and R.M.W. were supported by the Stanford University Vice Provost for Undergraduate Education through the Chemical Engineering Research Experience for Undergraduates program. We thank the Stanford Doerr School of Sustainability Accelerator for providing funding support to N.S. FTIR analysis was performed at the Stanford Synchrotron Radiation Lightsource at SLAC National Accelerator Laboratory, supported by the U.S. Department of Energy, Office of Science, Office of Basic Energy Sciences under Contract No. DE-AC02-76SF00515. N.S. was instrumental in preparing and providing insight into FTIR spectra interpretation. Tarpeh lab members H.D. and B.C. were crucial in aiding experimental formulation and data synthesis through their knowledge of ion exchange phenomena and metalligand complexes. We thank Kelly A. Harrison and all members of the Tarpeh lab for reviewing and editing an earlier version of this manuscript.

Supporting Information

The supporting information contains a schematic of the electrochemical water electrolysis process with stoichiometric reactions for OER and HER, composition of tested adsorption solutions, information on membrane properties, composition of solutions tested during no-resin cation migration experiments, schematic of zinc reloading experiment setup, pathways of zinc elution in

aqueous solutions, suggestions towards improved N removal and recovery, and calculations with

the Nernst-Planck equation.

References

- 621 (1) Bodirsky, B. L.; Popp, A.; Lotze-Campen, H.; Dietrich, J. P.; Rolinski, S.; Weindl, I.; 622 Schmitz, C.; Müller, C.; Bonsch, M.; Humpenöder, F.; Biewald, A.; Stevanovic, M. 623 Reactive Nitrogen Requirements to Feed the World in 2050 and Potential to Mitigate
- 624 Nitrogen Pollution. *Nat Commun* **2014**, *5* (1), 3858. https://doi.org/10.1038/ncomms4858.
- (2) Erisman, J. W.; Galloway, J. N.; Seitzinger, S.; Bleeker, A.; Dise, N. B.; Petrescu, A. M.
 R.; Leach, A. M.; De Vries, W. Consequences of Human Modification of the Global
 Nitrogen Cycle. *Phil. Trans. R. Soc. B* 2013, 368 (1621), 20130116.
 https://doi.org/10.1098/rstb.2013.0116.
- Kyriakou, V.; Garagounis, I.; Vourros, A.; Vasileiou, E.; Stoukides, M. An Electrochemical Haber-Bosch Process. *Joule* 2020, *4* (1), 142–158.
 https://doi.org/10.1016/j.joule.2019.10.006.
- (4) Miller, D. M.; Abels, K.; Guo, J.; Williams, K. S.; Liu, M. J.; Tarpeh, W. A.
 Electrochemical Wastewater Refining: A Vision for Circular Chemical Manufacturing. *J. Am. Chem. Soc.* 2023, *145* (36), 19422–19439. https://doi.org/10.1021/jacs.3c01142.
- Clark, B.; Sharma, N.; Apraku, E.; Dong, H.; Tarpeh, W. A. Ligand Exchange Adsorbents for Selective Phosphate and Total Ammonia Nitrogen Recovery from Wastewaters. *Acc. Mater. Res.* 2024. https://doi.org/10.1021/accountsmr.3c00290.
- 638 (6) Sengupta, S.; Nawaz, T.; Beaudry, J. Nitrogen and Phosphorus Recovery from Wastewater. 639 *Curr Pollution Rep* **2015**, *I* (3), 155–166. https://doi.org/10.1007/s40726-015-0013-1.
- 640 (7) Stein, L. Y.; Klotz, M. G. The Nitrogen Cycle. *Current Biology* **2016**, *26* (3), R94–R98. https://doi.org/10.1016/j.cub.2015.12.021.
- (8) Tansel, B. Significance of Thermodynamic and Physical Characteristics on Permeation of
 Ions during Membrane Separation: Hydrated Radius, Hydration Free Energy and Viscous
 Effects. Separation and Purification Technology 2012, 86, 119–126.
 https://doi.org/10.1016/j.seppur.2011.10.033.
- 646 (9) Malovanyy, A.; Sakalova, H.; Yatchyshyn, Y.; Plaza, E.; Malovanyy, M. Concentration of 647 Ammonium from Municipal Wastewater Using Ion Exchange Process. *Desalination* **2013**, 648 329, 93–102. https://doi.org/10.1016/j.desal.2013.09.009.
- (10) Clark, B.; Tarpeh, W. A. Selective Recovery of Ammonia Nitrogen from Wastewaters with
 Transition Metal-Loaded Polymeric Cation Exchange Adsorbents. *Chem. Eur. J.* 2020, 26
 (44), 10099–10112. https://doi.org/10.1002/chem.202002170.
- (11) Tarpeh, W. A.; Barazesh, J. M.; Cath, T. Y.; Nelson, K. L. Electrochemical Stripping to
 Recover Nitrogen from Source-Separated Urine. *Environ. Sci. Technol.* 2018, 52 (3), 1453–1460. https://doi.org/10.1021/acs.est.7b05488.
- (12) Tarpeh, W. A.; Chen, X. Making Wastewater Obsolete: Selective Separations to Enable
 Circular Water Treatment. *Environmental Science and Ecotechnology* 2021, 5, 100078.
 https://doi.org/10.1016/j.ese.2021.100078.

- (13) Dong, H.; Laguna, C. M.; Liu, M. J.; Guo, J.; Tarpeh, W. A. Electrified Ion Exchange
 Enabled by Water Dissociation in Bipolar Membranes for Nitrogen Recovery from Source Separated Urine. *Environ. Sci. Technol.* 2022, *56* (22), 16134–16143.
 https://doi.org/10.1021/acs.est.2c03771.
- (14) Clark, B.; Gilles, G.; Tarpeh, W. A. Resin-Mediated pH Control of Metal-Loaded Ligand
 Exchangers for Selective Nitrogen Recovery from Wastewaters. ACS Appl. Mater.
 Interfaces 2022, 14 (20), 22950–22964. https://doi.org/10.1021/acsami.1c22316.
- 665 (15) Gupta, G.; Torres, N. Use of Fly Ash in Reducing Toxicity of and Heavy Metals in Wastewater Effluent. *Journal of Hazardous Materials* **1998**, *57* (1), 243–248. https://doi.org/10.1016/S0304-3894(97)00093-9.
- (16) Lester, J. N. Significance and Behaviour of Heavy Metals in Waste Water Treatment
 Processes I. Sewage Treatment and Effluent Discharge. *Science of The Total Environment* 1983, 30, 1–44. https://doi.org/10.1016/0048-9697(83)90002-5.
- 671 (17) Qasem, N. A. A.; Mohammed, R. H.; Lawal, D. U. Removal of Heavy Metal Ions from Wastewater: A Comprehensive and Critical Review. *npj Clean Water* **2021**, *4* (1), 1–15. https://doi.org/10.1038/s41545-021-00127-0.
- (18) Kogler, A.; Farmer, M.; Simon, J. A.; Tilmans, S.; Wells, G. F.; Tarpeh, W. A. Systematic
 Evaluation of Emerging Wastewater Nutrient Removal and Recovery Technologies to
 Inform Practice and Advance Resource Efficiency. ACS EST Eng. 2021, 1 (4), 662–684.
 https://doi.org/10.1021/acsestengg.0c00253.
- (19) Kogler, A.; Sharma, N.; Tiburcio, D.; Gong, M.; Miller, D. M.; Williams, K. S.; Chen, X.;
 Tarpeh, W. A. Long-Term Robustness and Failure Mechanisms of Electrochemical
 Stripping for Wastewater Ammonia Recovery. ACS Environ. Au 2024.
 https://doi.org/10.1021/acsenvironau.3c00058.
- 682 (20) Bauschlicher, C. W., Jr. Transition Metal–Ligand Bonding. II. *The Journal of Chemical Physics* **1986**, *84* (1), 260–267. https://doi.org/10.1063/1.450179.
- (21) Mustafa, S.; Nadia, L. H.; Rehana, N.; Naeem, A.; Samad, H. Y. Ligands Sorption Studies
 on Transition Metal Ion Loaded Amberlite IRC-50. *Langmuir* 1998, 14 (9), 2378–2384.
 https://doi.org/10.1021/la9706328.
- 687 (22) Irving, H.; Williams, R. J. P. 637. The Stability of Transition-Metal Complexes. *J. Chem. Soc.* **1953**, No. 0, 3192–3210. https://doi.org/10.1039/JR9530003192.
- 689 (23) Wang, H.; Zeuschner, J.; Eremets, M.; Troyan, I.; Willams, J. Stable Solid and Aqueous 690 H2CO3 from CO2 and H2O at High Pressure and High Temperature. *Sci Rep* **2016**, *6* (1), 691 19902. https://doi.org/10.1038/srep19902.
- 692 (24) Liu, M. J.; Miller, D. M.; Tarpeh, W. A. Reactive Separation of Ammonia from Wastewater 693 Nitrate via Molecular Electrocatalysis. *Environ. Sci. Technol. Lett.* **2023**, 694 acs.estlett.3c00205. https://doi.org/10.1021/acs.estlett.3c00205.
- 695 (25) Liu, M. J.; Neo, B. S.; Tarpeh, W. A. Building an Operational Framework for Selective 696 Nitrogen Recovery via Electrochemical Stripping. *Water Research* **2020**, *169*, 115226. 697 https://doi.org/10.1016/j.watres.2019.115226.
- (26) Wang, W.; Zhang, Y.; Tan, M.; Xue, C.; Zhou, W.; Bao, H.; Hon Lau, C.; Yang, X.; Ma, J.;
 Shao, L. Recent Advances in Monovalent Ion Selective Membranes towards Environmental
 Remediation and Energy Harvesting. Separation and Purification Technology 2022, 297,
 121520. https://doi.org/10.1016/j.seppur.2022.121520.

- 702 (27) Rehman, D.; Ahdab, Y. D.; Lienhard, J. H. Monovalent Selective Electrodialysis:
 703 Modelling Multi-Ionic Transport across Selective Membranes. Water Research 2021, 199,
 704 117171. https://doi.org/10.1016/j.watres.2021.117171.
- 705 (28) Huang, J. H.; Cheng, X. Q.; Wu, Y. D.; Zhang, Y. Q.; Li, S. W.; Lau, C. H.; Shao, L. Critical Operation Factors and Proposed Testing Protocol of Nanofiltration Membranes for Developing Advanced Membrane Materials. *Adv Compos Hybrid Mater* **2021**, *4* (4), 1092–1101. https://doi.org/10.1007/s42114-021-00334-w.
- (29) Goldin, M. M.; Khubutiya, M. Sh.; Kolesnikov, V. A.; Abakumov, M. M.; Evseev, A. K.;
 Volkov, A. G. Indirect Electrochemical Synthesis of Active Oxygen in Dilute Sulfate
 Solutions. *J Appl Electrochem* 2009, *39* (2), 185–189. https://doi.org/10.1007/s10800-008-9652-x.
- 713 (30) Liu, Z.; Wang, Y.; Li, Y.; Chang, H. Electro-Assisted Regeneration of Ion Exchange
 714 Resins. *Front. Environ. Sci. Eng. China* 2008, 2 (4), 410–414.
 715 https://doi.org/10.1007/s11783-008-0069-x.
- 716 (31) Kim, K.-W.; Kim, Y.-J.; Kim, I.-T.; Park, G.-I.; Lee, E.-H. Electrochemical Conversion 717 Characteristics of Ammonia to Nitrogen. *Water Research* **2006**, *40* (7), 1431–1441. 718 https://doi.org/10.1016/j.watres.2006.01.042.
- 719 (32) Ran, J.; Wu, L.; He, Y.; Yang, Z.; Wang, Y.; Jiang, C.; Ge, L.; Bakangura, E.; Xu, T. Ion
 720 Exchange Membranes: New Developments and Applications. *Journal of Membrane*721 *Science* **2017**, *522*, 267–291. https://doi.org/10.1016/j.memsci.2016.09.033.
- 722 (33) Dong, H.; Wei, L.; Tarpeh, W. A. Electro-Assisted Regeneration of pH-Sensitive Ion 723 Exchangers for Sustainable Phosphate Removal and Recovery. *Water Research* **2020**, *184*, 724 116167. https://doi.org/10.1016/j.watres.2020.116167.
- 725 (34) Rodrigues, M.; Sleutels, T.; Kuntke, P.; Buisman, C. J. N.; Hamelers, H. V. M. Effects of Current on the Membrane and Boundary Layer Selectivity in Electrochemical Systems
 727 Designed for Nutrient Recovery. *ACS Sustainable Chem. Eng.* **2022**, *10* (29), 9411–9418.
 728 https://doi.org/10.1021/acssuschemeng.2c01764.
- 729 (35) Hamm, L. L.; Simon, E. E. Roles and Mechanisms of Urinary Buffer Excretion. *Am J Physiol* **1987**, *253* (4 Pt 2), F595-605. https://doi.org/10.1152/ajprenal.1987.253.4.F595.
- (36) Pismenskaya, N.; Laktionov, E.; Nikonenko, V.; El Attar, A.; Auclair, B.; Pourcelly, G.
 Dependence of Composition of Anion-Exchange Membranes and Their Electrical
 Conductivity on Concentration of Sodium Salts of Carbonic and Phosphoric Acids. *Journal* of Membrane Science 2001, 181 (2), 185–197. https://doi.org/10.1016/S0376 7388(00)00529-9.
- 736 (37) Mesmer, R. E.; Baes, C. F. Review of Hydrolysis Behavior of Ions in Aqueous Solutions.
 737 MRS Online Proceedings Library 1990, 180 (1), 85. https://doi.org/10.1557/PROC-180-85.
- (38) McEnaney, J. M.; Blair, S. J.; Nielander, A. C.; Schwalbe, J. A.; Koshy, D. M.; Cargnello,
 M.; Jaramillo, T. F. Electrolyte Engineering for Efficient Electrochemical Nitrate Reduction
 to Ammonia on a Titanium Electrode. ACS Sustainable Chem. Eng. 2020, 8 (7), 2672–
 2681. https://doi.org/10.1021/acssuschemeng.9b05983.
- 742 (39) Dinh, H. Q.; Toh, W. L.; Chu, A. T.; Surendranath, Y. Neutralization Short-Circuiting with
 743 Weak Electrolytes Erodes the Efficiency of Bipolar Membranes. ACS Appl. Mater.
 744 Interfaces 2023, acsami.2c18685. https://doi.org/10.1021/acsami.2c18685.
- 745 (40) Zhang, L.; Shi, Z.; Lin, Y.; Chong, F.; Qi, Y. Design Strategies for Large Current Density
 746 Hydrogen Evolution Reaction. *Frontiers in Chemistry* 2022, 10.

- 747 (41) Boettcher, S. W.; Oener, S. Z.; Lonergan, M. C.; Surendranath, Y.; Ardo, S.; Brozek, C.; 748 Kempler, P. A. Potentially Confusing: Potentials in Electrochemistry. *ACS Energy Lett.* 749 **2021**, *6* (1), 261–266. https://doi.org/10.1021/acsenergylett.0c02443.
- (42) Oelßner, W. Cell, Electrochemical. In *Encyclopedia of Applied Electrochemistry*; Kreysa,
 G., Ota, K., Savinell, R. F., Eds.; Springer: New York, NY, 2014; pp 163–170.
 https://doi.org/10.1007/978-1-4419-6996-5 433.
- 753 (43) Tarpeh, W. A.; Barazesh, J. M.; Cath, T. Y.; Nelson, K. L. Electrochemical Stripping to 754 Recover Nitrogen from Source-Separated Urine. *Environ. Sci. Technol.* **2018**, *52* (3), 1453– 755 1460. https://doi.org/10.1021/acs.est.7b05488.
- 756 (44) Matsumoto, H.; Tanioka, A.; Murata, T.; Higa, M.; Horiuchi, K. Effect of Proton on 757 Potassium Ion in Countertransport across Fine Porous Charged Membranes. *J. Phys. Chem.* 758 *B* **1998**, *102* (25), 5011–5016. https://doi.org/10.1021/jp972223q.
- 759 (45) Tang, C.; Yaroshchuk, A.; Bruening, M. L. Flow through Negatively Charged, Nanoporous 760 Membranes Separates Li+ and K+ Due to Induced Electromigration. *Chem. Commun.* **2020**, 761 56 (74), 10954–10957. https://doi.org/10.1039/D0CC03143G.
- (46) Moshtarikhah, S.; Oppers, N. A. W.; de Groot, M. T.; Keurentjes, J. T. F.; Schouten, J. C.;
 van der Schaaf, J. Nernst–Planck Modeling of Multicomponent Ion Transport in a Nafion
 Membrane at High Current Density. *J Appl Electrochem* 2017, 47 (1), 51–62.
 https://doi.org/10.1007/s10800-016-1017-2.
- (47) Sujanani, R.; Nordness, O.; Miranda, A.; Katz, L. E.; Brennecke, J. F.; Freeman, B. D.
 Accounting for Ion Pairing Effects on Sulfate Salt Sorption in Cation Exchange
 Membranes. *J. Phys. Chem. B* 2023, *127* (8), 1842–1855.
 https://doi.org/10.1021/acs.jpcb.2c07900.
- (48) del Rosario, J. A. D.; Li, G.; Labata, M. F. M.; Ocon, J. D.; Chuang, P.-Y. A. Unravelling
 the Roles of Alkali-Metal Cations for the Enhanced Oxygen Evolution Reaction in Alkaline
 Media. *Applied Catalysis B: Environmental* 2021, 288, 119981.
 https://doi.org/10.1016/j.apcatb.2021.119981.
- 774 (49) Palacios, E. G.; Juárez-López, G.; Monhemius, A. J. Infrared Spectroscopy of Metal 775 Carboxylates. *Hydrometallurgy* **2004**, *72* (1–2), 139–148. https://doi.org/10.1016/S0304-776 386X(03)00137-3.
- 777 (50) Max, J.-J.; Chapados, C. Infrared Spectroscopy of Aqueous Carboxylic Acids: Comparison 778 between Different Acids and Their Salts. *J. Phys. Chem. A* **2004**, *108* (16), 3324–3337. 779 https://doi.org/10.1021/jp036401t.
- 780 (51) Liu, Y.; Qin, M.; Luo, S.; He, Z.; Qiao, R. Understanding Ammonium Transport in Bioelectrochemical Systems towards Its Recovery. *Sci Rep* **2016**, *6* (1), 22547. https://doi.org/10.1038/srep22547.
- 783 (52) Epsztein, R.; Shaulsky, E.; Qin, M.; Elimelech, M. Activation Behavior for Ion Permeation
 784 in Ion-Exchange Membranes: Role of Ion Dehydration in Selective Transport. *Journal of Membrane Science* 2019, 580, 316–326. https://doi.org/10.1016/j.memsci.2019.02.009.
- 786 (53) Richards, L. A.; Schäfer, A. I.; Richards, B. S.; Corry, B. The Importance of Dehydration in Determining Ion Transport in Narrow Pores. *Small* **2012**, *8* (11), 1701–1709. https://doi.org/10.1002/smll.201102056.
- 789 (54) Dietrich, A. M.; Burlingame, G. A. Critical Review and Rethinking of USEPA Secondary
 790 Standards for Maintaining Organoleptic Quality of Drinking Water. *Environ. Sci. Technol.* 791 2015, 49 (2), 708–720. https://doi.org/10.1021/es504403t.

- 792 (55) Kitchen, D. B.; Allen, L. C. Zinc Complexes of Water, Hydroxide, and Ammonia. *J. Phys. Chem.* **1989**, *93* (20), 7265–7269. https://doi.org/10.1021/j100357a046.
- 794 (56) Krężel, A.; Maret, W. The Biological Inorganic Chemistry of Zinc Ions. *Archives of Biochemistry and Biophysics* **2016**, *611*, 3–19. https://doi.org/10.1016/j.abb.2016.04.010.
- 796 (57) Muddemann, T.; Haupt, D.; Sievers, M.; Kunz, U. Electrochemical Reactors for Wastewater Treatment. *ChemBioEng Reviews* **2019**, *6* (5), 142–156. https://doi.org/10.1002/cben.201900021.
- (58) Meese, A. F.; Kim, D. J.; Wu, X.; Le, L.; Napier, C.; Hernandez, M. T.; Laroco, N.;
 Linden, K. G.; Cox, J.; Kurup, P.; McCall, J.; Greene, D.; Talmadge, M.; Huang, Z.;
 Macknick, J.; Sitterley, K. A.; Miara, A.; Evans, A.; Thirumaran, K.; Malhotra, M.;
 Gonzalez, S. G.; Rao, P.; Stokes-Draut, J.; Kim, J.-H. Opportunities and Challenges for
 Industrial Water Treatment and Reuse. ACS EST Eng. 2022, 2 (3), 465–488.
 https://doi.org/10.1021/acsestengg.1c00282.
- Kato, T.; Kuroda, H.; Nakasone, H. Runoff Characteristics of Nutrients from an
 Agricultural Watershed with Intensive Livestock Production. *Journal of Hydrology* 2009,
 368 (1), 79–87. https://doi.org/10.1016/j.jhydrol.2009.01.028.
- 808 (60) Lang, M.; Li, P.; Yan, X. Runoff Concentration and Load of Nitrogen and Phosphorus from a Residential Area in an Intensive Agricultural Watershed. *Science of The Total Environment* **2013**, *458–460*, 238–245. https://doi.org/10.1016/j.scitotenv.2013.04.044.
- (61) Meerbergen, K.; Van Geel, M.; Waud, M.; Willems, K. A.; Dewil, R.; Van Impe, J.;
 Appels, L.; Lievens, B. Assessing the Composition of Microbial Communities in Textile
 Wastewater Treatment Plants in Comparison with Municipal Wastewater Treatment Plants.
 MicrobiologyOpen 2017, 6 (1), e00413. https://doi.org/10.1002/mbo3.413.
- (62) Mendoza Grijalva, L.; Brown, B.; Cauble, A.; Tarpeh, W. A. Diurnal Variability of SARS-CoV-2 RNA Concentrations in Hourly Grab Samples of Wastewater Influent during Low COVID-19 Incidence. ACS EST Water 2022, 2 (11), 2125–2133.
 https://doi.org/10.1021/acsestwater.2c00061.